Photonic crystal disk lasers

Yinan Zhang,[1,*] Christoph Hamsen,[1,3] Jennifer T. Choy,[1] Yong Huang,[2] Jae-Hyun Ryou,[2] Russell D. Dupuis,[2] and Marko Loncar[1]

[1]*School of Engineering and Applied Sciences, Harvard University, 9 Oxford Street, Cambridge, Massachusetts 02138, USA*

[2]*School of Electrical and Computer Engineering, Georgia Institute of Technology, 777 Atlantic Drive NW, Atlanta, Georgia 30332-0250, USA*

[3]*Department of Physics, Technische Universität München, James-Franck-Strasse 1, 85748 Garching, Germany*

**Corresponding author: yinan@seas.harvard.edu*

Received April 29, 2011; revised June 22, 2011; accepted June 22, 2011; posted June 22, 2011 (Doc. ID 146870); published July 14, 2011

A novel type of nanolasers, which combines the advantages of photonic crystal lasers and microdisk lasers, has been demonstrated based on InAlGaAs/InGaAs quantum wells using pulsed optical pumping at room temperature. It incorporates the properties of small footprint, small mode volume, and submilliwatt threshold, and favors vertical emission. We believe that this type of laser acts as a promising candidate for highly-integrated on-chip nanolasers in applications for signal processing and index sensing.

OCIS codes: 140.3945, 050.5298, 140.3410.

The ultimate nanolaser would have a device footprint of the order of an optical wavelength in all three dimensions, a low power consumption (lasing threshold) that requires a small modal volume (V_{mod}) and a high Q factor, and a high extraction efficiency. Photonic crystal lasers and microdisk lasers are two candidate solutions toward reaching these goals.

Photonic crystal lasers [1,2] are capable of confining photons within a modal volume close to the diffraction limit [$\sim(\lambda/n)^3$]. These properties have been proven to make nanolaser devices with low threshold [3,4] and high modulation speed [5,6] feasible. In addition, photonic crystal lasers can be tailored to emit vertically by engineering the pattern of the cavity mode [7]. Despite these properties, photonic crystal lasers have a few drawbacks. First, the footprint of the photonic crystal lasers is limited by the multiple periodic Bragg layers used to confine the cavity mode. Second, most photonic crystal cavities rely on suspended semiconductor membranes to provide a good index contrast, which makes efficient electrical injection of carriers into the cavity mode difficult. Microdisk lasers [8], on the other hand, rely on whispering gallery mode pinned via total internal reflection to the boundary of the disk. They offer a platform for very compact electrically driven lasers, with a footprint of the order of optical wavelength [9–11]. However, the whispering gallery mode travels through the whole circular edge of the microdisk and therefore results in a relatively large mode volume [Fig. 1(c)]. Furthermore, the whispering gallery mode does not emit vertically, which makes the collection of photons difficult [12]. Normally, evanescent coupling via a tapered fiber is used to collect the emitted photons efficiently [9]. This makes integration of large arrays of microdisk lasers problematic. To overcome this, a vertically emitting microdisk laser uses a second-order metallic grating atop to extract the light [13].

In this Letter, we demonstrate nanolasers operated at room temperature based on a novel type of nanocavities, which combines the properties of microdisk and photonic crystal lasers. It incorporates an array of holes at the perimeter of the microdisk in order to confine the whispering gallery mode in a limited angular range within a small mode volume. The design can also be understood as a photonic crystal nanobeam cavity [Fig. 1(d)] [14–16] bent into a disk [Fig. 1(a)]. In this way, Bragg mirrors at each end of the nanobeam are combined in one curved Bragg mirror. Therefore, the number of holes can be decreased because the transmission losses are cycled through the disk, which reduces the device footprint.

We start our design with a 2.56 μm diameter, 325 nm thick microdisk that supports a resonance of $\mathrm{TE}_{1,10}$ mode at 1750 nm. Next, we add 20 holes with equal angular spacing around the perimeter of the disk. This causes the two degenerate $\mathrm{TE}_{1,10}$ modes, which propagate in clockwise and counterclockwise directions, to split into two standing wave modes: one mode with its field concentrated in the dielectric and the other concentrated in the hole region, as shown in Figs. 2(b) and 2(c). These modes are similar to the modes of microgear cavities [17]. Analogous to photonic crystals, these two modes correspond to the dielectric band edge and air band edge. Between these band edges, the propagation of the $\mathrm{TE}_{1,10}$ mode is forbidden. In order to maximize the bandgap width and thereby optimize the azimuthal confinement, we place the center of the holes at the electric field maximum. Figure 2(a) shows the band edge wavelength and normalized bandgap width (ratio of the gap width to the midgap wavelength) as a function of the hole radius. It can be seen that the bandgap is maximized at 97 nm and the center of the bandgap is at ~1550 nm.

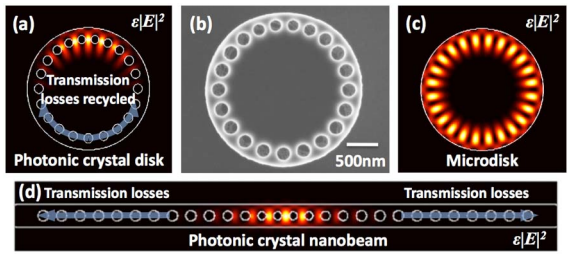

Fig. 1. (Color online) (a) Schematic of photonic crystal disk laser and (b) fabricated photonic crystal disk laser. The device can be viewed as a hybrid between (c) microdisk laser and (d) photonic crystal nanobeam laser with photonic crystal folded back to minimize the transmission losses.

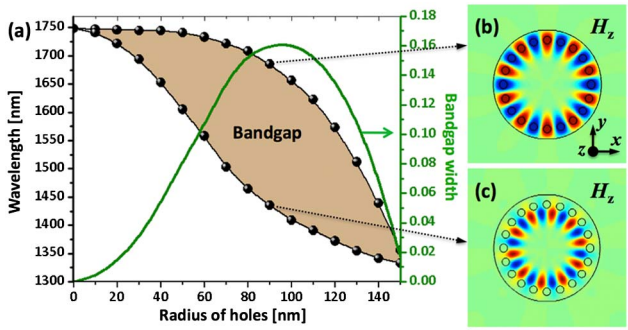

Fig. 2. (Color online) (a) Band edge wavelength as a function of the radius of holes on photonic crystal disk (black dots), with the bandgap shaded in bronze. The green (solid) curve shows the corresponding normalized bandgap width. (b),(c) Resonant mode profiles at the band edge of the H_z component for dielectric band and air band mode, respectively.

We emphasize that the bandgap is not complete: there are higher-order modes with different radial field distribution that may exist in the wavelength of interest.

Next, we introduce the defect region to the disk by modifying the hole-to-hole angular spacing as well as the holes' radii. The final structure is shown in Fig. 1(b), where there are 11 identical holes on the bottom half acting as Bragg mirrors and 10 tapered holes on the top half to localize the mode while suppressing the scattering losses [18]. The cavity mode resonates at 1546 nm and, without considering material losses, has a Q factor of 1.0×10^5 and a modal volume of $0.52(\lambda/n)^3$. The mode volume is on the same order of photonic crystal nanobeam cavities [14–16].

Our cavities are fabricated on commercial InP substrate. A 325 nm thick $In_{0.53}(Al_{0.4}Ga_{0.6})_{0.47}As$ layer is epitaxially grown atop using metal–organic chemical vapor deposition. It contains four compressively strained $In_{0.58}Ga_{0.42}As$ quantum wells, which support TE-polarized gain covering the wavelength range from 1480 to 1650 nm. The pattern is defined with electron beam lithography. The pattern is subsequently transferred to the $In_{0.53}(Al_{0.4}Ga_{0.6})_{0.47}As$ slab and InP substrate with inductively coupled plasma reactive ion etching. The disk structure is finally realized by selectively wet etching the mesa with 3:1 $HCl:H_2O$ solution [Fig. 3(a)]. We also fabricate a microdisk without perforated holes with the same diameter to compare the results [Fig. 3(b)]. The two arrays are scaled linearly in size to vary the cavities' resonant wavelengths.

The devices are optically pumped at room temperature using a 980 nm semiconductor laser with 10 ns pulses and 400 kHz repetition rate. The pump beam is focused to a 3 μm diameter spot using a 100× objective lens. The effective pump power is estimated with power measurement after the objective while taking into account the spatial overlap between the pump beam and the lasing mode. The emission beam is collected through the same objective lens from the top and analyzed with an InGaAs detector filtered by a monochromator.

For both photonic crystal disks and microdisks, Fig. 3(e) depicts the lasing wavelength as a function of the diameter of the disk, Figs. 3(c) and 3(d) are photonic crystal disk modes, and Figs. 3(f) and 3(g) are microdisk modes. It shows good agreement with the simulation results plotted in solid lines, which verifies the lasing mode

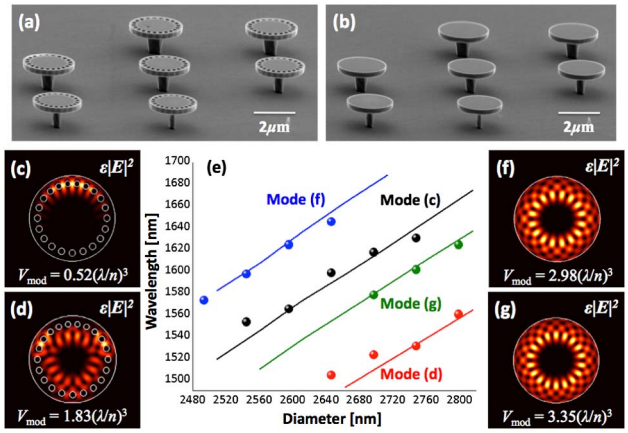

Fig. 3. (Color online) (a),(b) Images of photonic crystal disk and microdisk lasers with different scaling factors. (c),(d) Electric field density profiles of photonic crystal disk modes. (e) Experimental results of lasing wavelength dependence on diameter of photonic crystal disks (black (second highest) dots and red (lowest) dots) and microdisks (blue (highest) dots and green (second lowest) dots). The solid curves show the mode wavelength dependence obtained using simulations. (f),(g) Electric field density profiles of microdisk modes.

in Fig. 3(c) is of the designed defect mode. We note that by controlling the position of the pump spot, lasing from two different photonic crystal disk modes could be obtained in some structures [Fig. 3(e)]. The nanolaser, however, does operate in a single-mode regime in both cases (only one mode lases at one time). We also note that the two microdisk lasing modes are not the fundamental $TE_{1,m}$ modes, but the higher-order $TE_{2,8}$ and $TE_{2,9}$ modes. These modes have a node of electric field in the radial direction. The fundamental modes cannot be collected from the top because it emits in in-plane directions [12].

Next, we study the properties of the designed photonic crystal disk mode from one single device [Fig. 4(a)]. Figure 4(b) shows the lasing power as a function of the effective pump power (also known as an L–L curve) in comparison with a microdisk laser emitting at the same wavelength. The injection efficiencies are estimated to be 1.74% and 4.36% for the photonic crystal disk mode and microdisk mode, respectively. From Fig. 4(b), the photonic crystal disk lasers have much better extraction efficiencies than microdisk lasers. We believe that this efficiency can be further boosted with subtle far-field engineering of photonic crystals [7]. The inset plots the spectrum at 3.2 times the threshold power of the photonic crystal disk mode, which shows a clear single-mode lasing emission. In Fig. 4(c) we plot the L–L curve for the photonic crystal disk laser in log–log scale (black dots), along with the L–L curves obtained from rate equations for different spontaneous emission factors (β). The experimental data show good agreement with a β factor of 0.087. More than a tenfold reduction in β factor of this laser compared to a nanobeam laser [14] can be attributed to the existence of higher-order modes. In Fig. 4(d), we show the lasing spectrum of the photonic crystal disk lasers slightly above the lasing threshold (1.1 × threshold). It has an FWHM of 0.26 nm, which corresponds to a Q factor of ~6000. The Q factor is limited by

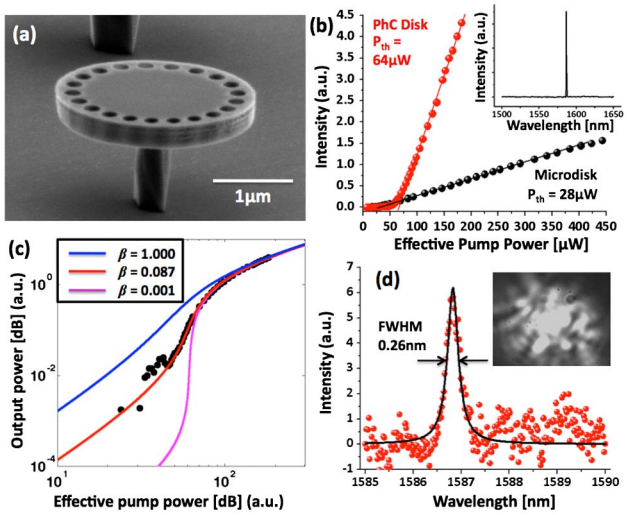

Fig. 4. (Color online) (a) Images of fabricated photonic crystal disk from scanning electron microscope. (b) Light-in light-out curve for photonic crystal disk laser and microdisk laser, respectively. Inset shows the spectrum of photonic crystal disk lasers at 3.2× lasing threshold. (c) Log–log plot of the photonic crystal disk laser's L–L curve (black-dots). The solid curves show L–L curves deduced from rate equations with different β factors. (d) Line shape of the lasing mode above threshold (red dots), fitted with a Lorentzian line function (solid red). Inset shows the emission profile taken from an infrared camera.

the resolution of the monochromator. Free-carrier absorption is also known to decrease the Q factor extensively below its passive value [9]. We also show the lasing emission profile of the photonic crystal disk laser in the inset of Fig. 4(d), which is taken from a near-infrared camera. Finally, we note that the linewidth narrowing effect above the threshold could not be observed due to the strong heating effects in nanolasers, as previously reported [15].

In summary, we have demonstrated a novel type of photonic crystal lasers that takes advantage of both microdisk and photonic crystal geometries and has a small footprint, small mode volume, and high extraction efficiency.

This work was supported in part by National Science Foundation (NSF) grant ECCS-1028519, "Collaborative Research: Nanobeam Lasers." The authors acknowledge the support provided by the Center for Nanoscale Systems (CNS) at Harvard University. Y. Zhang would like to dedicate this paper to Mehmet Dundar.

References

1. O. Painter, R. K. Lee, A. Scherer, A. Yariv, J. D. O'Brien, P. D. Dapkus, and I. Kim, Science **284**, 1819 (1999).
2. H. G. Park, S. H. Kim, S. H. Kwon, Y. G. Ju, J. K. Yang, J. H. Baek, S. B. Kim, and Y. H. Lee, Science **305**, 1444 (2004).
3. L. J. Martinez, B. Alen, I. Prieto, D. Fuster, L. Gonzalez, Y. Gonzalez, M. L. Dotor, and P. A. Postigo, Opt. Express **17**, 14993 (2009).
4. K. Nozaki, S. Kita, and T. Baba, Opt. Express **15**, 7506 (2007).
5. H. Altug, D. Englund, and J. Vuckovic, Nat. Phys. **2**, 484 (2006).
6. S. Matsuo, A. Shinya, T. Kakitsuka, K. Nozaki, T. Segawa, T. Sato, Y. Kawaguchi, and M. Notomi, Nat. Photonics **4**, 648 (2010).
7. S. H. Kim, S. K. Kim, and Y. H. Lee, Phys. Rev. B **73**, 235117 (2006).
8. S. L. McCall, A. F. J. Levi, R. E. Slusher, S. J. Pearton, and R. A. Logan, Appl. Phys. Lett. **60**, 289 (1992).
9. M. Fujita, A. Sakai, and T. Baba, IEEE J. Sel. Top. Quantum Electron. **5**, 673 (1999).
10. Z. Liu, J. M. Shainline, G. E. Fernandes, J. Xu, J. Chen, and C. F. Gmachl, Opt. Express **18**, 19242 (2010).
11. A. F. J. Levi, R. E. Slusher, S. L. McCall, T. Tanbun-Ek, D. L. Coblentz, and S. J. Pearton, Electron. Lett. **28**, 1010 (1992).
12. T. D. Lee, P. H. Cheng, J. S. Pan, R. S. Tsai, Y. Lai, and K. Tai, Appl. Phys. Lett. **72**, 2223 (1998).
13. L. Mahler, A. Tredicucci, F. Beltram, C. Walther, J. Faist, B. Witzigmann, H. E. Beere, and D. A. Ritchie, Nat. Photonics **3**, 46 (2008).
14. Y. Zhang, M. Khan, Y. Huang, J. Ryou, P. Deotare, R. Dupuis, and M. Loncar, Appl. Phys. Lett. **97**, 051104 (2010).
15. Y. Gong, B. Ellis, G. Shambat, T. Sarmiento, J. S. Harris, and J. Vuckovic, Opt. Express **18**, 8781 (2010).
16. B. H. Ahn, J. H. Kang, M. K. Kim, J. H. Song, B. Min, K. S. Kim, and Y. H. Lee, Opt. Express **18**, 5654 (2010).
17. M. Fujita and T. Baba, Appl. Phys. Lett. **80**, 2051 (2002).
18. Y. Zhang and M. Loncar, Opt. Express **16**, 17400 (2008).